Available online at www.sciencedirect.com
ScienceDirect
Pattern Recognition 41 (2008) 3035 – 3043
PATTERN RECOGNITION
THE JOURNAL OF THE PATTERN RECOGNITION SOCIETY
www.elsevier.com/locate/pr

A segmentation algorithm for SAR images based on the anisotropic heat diffusion equation

Gui Gao[a,*], Lingjun Zhao[a], Jun Zhang[a], Diefei Zhou[b], Jijun Huang[a]

[a]National University of Defence Technology, Changsha 410073, China
[b]Hunan Normal University, Changsha 410081, China

Received 8 July 2006; received in revised form 25 January 2008; accepted 31 January 2008

Abstract

A method toward unsupervised segmentation of synthetic aperture radar (SAR) images is proposed. In this method, the distribution of SAR intensity image and the maximum a posteriori (MAP) algorithm is used to obtain an initial segmentation. Then according to the equivalence between the solid heat diffusion model and image scale-space, multiscale anisotropic smoothing of the posterior probability matrixes is introduced to remove the influence of speckle and to preserve important structure information. The effectiveness of this algorithm is demonstrated by application to simulated and real SAR images.

Keywords: Synthetic aperture radar (SAR) image; Segmentation; Maximum a posteriori (MAP); Anisotropic diffusion (AD)

1. Introduction

The segmentation of synthetic aperture radar (SAR) images has received an increasing amount of attention from the image processing community [1]. Many segmentation approaches for SAR images have been proposed over the last few years [2–16]. They can be divided into two classes, namely, (1) speckle noise filtering is performed on raw SAR images followed by a segmentation scheme similar to segmentation for optical images [2–4]; (2) speckle reduction is integrated into the segmentation process, making use of the intensity and structure information of pixels in SAR images. Although the former is simple, compared with the latter, it has two disadvantages. Firstly, better segmentation tends to be obtained on images with large looks when using the first class of segmentation approaches. If SAR images are corrupted by strong speckle, strong filtering is required to minimize the influence of the speckle, which usually deteriorates the performance of segmentation. Moreover, it is difficult to control the extent of speckle filtering for high-quality segmentation. Secondly, a speckle filter with good performance often introduces complex computation which may lead to the inefficiency of the whole process.

Based on the problems mentioned above, recent researches on SAR image segmentation mainly focus on integrating speckle reduction into the segmentation process (see Refs. [5–18]). Many segmentation approaches of SAR images in this category have been reported in the literature. Lombardo [14] proposed a statistically optimal segmentation scheme based on a generalized maximum likelihood (ML) approach for polarimetric land applications. This technique is developed from the work of Lombardo and Oliver [15,16]. It can be divided into two steps: (1) the ML approach, exploiting the statistical behavior of SAR image, is used to segment the image into regions with homogeneous characteristics; (2) a split–merge test utilizing the structural information of the image is implemented to produce final segmentation and reduce the speckle noise at the same time. The drawback of this method is that it uses simulated annealing (SA) to maximize the objective function estimating the unknown covariance matrix, and consequently the computation time required is significant. Additionally, an alternative approach, also reported in Ref. [14], based on the eigenvalues from polarimetric decomposition, has a much lower computation time. Anyway, the processing, consisting of

* Corresponding author. Tel.: +86 731 4573479.
E-mail address: dellar@126.com (G. Gao).

0031-3203/$30.00 © 2008 Elsevier Ltd. All rights reserved.
doi:10.1016/j.patcog.2008.01.029

two basic step and combining the statistical property and structural or spatial information of the image, has been a traditional and important idea for improving the segmentation performance of SAR images [14].

The Markov random field (MRF) model is probably one of the most popular tools for incorporating the spatial dependence among pixels into the segmentation [6–11]. Several attempts based on MRF have been made, such as the iterative conditional models (ICM) algorithm [10], the maximization of posterior marginals (MPM) method [13], and the SA approach [6]. Results from these methods are encouraging, but MRF models introduce parameters which cannot be easily determined and may lead to difficult optimization problems. Stewart et al. [11] used a two-term objective function that balances a statistical likelihood with a boundary smoothness constraint to increase the segmentation accuracy on SAR image. This task was framed as an optimization problem and found a minimum by SA in the objective function over the solution space. Their results look very good. Unfortunately, since the convergence rate of SA can be slow, the time-consumption problem still remains in practice. Recently, Deng and Clausi [9] presented a novel MRF-based segmentation algorithm, which adopts the widely used maximum a posteriori (MAP)–MRF framework. In this study, segmentation problem was formulated as maximizing the product of a conditional probability and a prior probability. The conditional probability is determined by feature information, and the prior probability is calculated with spatial information. Without the prior probability, this approach will degenerate into a simplified expectation-maximization (EM) algorithm, which heavily depends on initializations and is more vulnerable to trap to a local maximum. As a result, this approach sometimes fails to give a reasonable segmentation and thus has a poor average performance.

Another noticeable approach is based on nonlinear heat diffusion equation (anisotropic diffusion, AD), which surpasses most other techniques in accuracy and robustness [12]. This technique originates from the work of Perona and Malik [21], and falls into the category of partial differential equation (PDE) based image processing. Over the last few years, various AD-based speckle suppression methods for SAR images have been reported in the literature (see Refs. [17,19]), which demonstrate the AD-based methods have good performance of de-speckling. Typically, to suppress speckle while preserving edge information, Yu and Acton [17] introduced an edge sensitive diffusion method, called speckle reducing anisotropic diffusion (SRAD), which defined an instantaneous coefficient of variation as the edge detector for speckled imagery. This method is further developed by Aja-Fernández and Alberola-López [19]. They analyzed a new AD filter based on Kuan's filter compared with the SRAD based on Lee and Frost filters. Both of the two methods can preserve or even enhance prominent edges when removing speckle. However, they also have the drawbacks of blurring and even eradicating detailed features of the image. Since the AD-based technique has a good de-speckling performance, it has been also applied to the segmentation of SAR images in recent years. Haker et al. [12] proposed a knowledge-based algorithm (also reported by Georgiou and Tannenbaum [18]) combining the Bayesian paradigm (exploiting the statistical behavior of the image) and AD (utilizing the spatial information of the image). Assuming that each class of object follows a normal distribution with two parameters (i.e. mean and standard deviation), they introduced a priori knowledge that the parameters of normal distribution are known or achieved by an offline training phase from a set of sample images. In this way, posterior probabilities are then obtained via Bayes' rule and smoothed several times by AD filter that is not limited to any special selection. The final segmentation is obtained by MAP classification of smoothed posterior probabilities. The results of segmenting the moving and stationary target acquisition and recognition (MSTAR) [20] SAR images show the good performance of this technique. But the offline training (sometimes one need to manually segment a few sample images [12]) to acquire the priori knowledge cannot adapt to user's need, and it is very specific to the application at hand, hence hard to be generalized into other domains. So it is in essence a supervised method and also has a limit in practicality.

From a practical point of view, this study focuses on developing a method toward unsupervised segmentation of SAR images. Considering the good de-speckling performance of the AD-based segmentation and its dependence on prior knowledge, we introduce a MAP [1,14–16] initial segmentation combining negative exponential distribution of SAR intensity image before the AD-based segmentation. Similar to the previous techniques (e.g. the work of Lombardo and Oliver [14–16]), our method mainly consists of two steps: the initial segmentation and speckle removal combining statistical and structural information. Firstly, MAP is applied to get an initial segmentation by classifying each pixel of the image automatically, as a priori knowledge of AD, and then the posterior probability matrix of each class is derived from the initial segmentation. Secondly, multiscale smoothing according to AD first described by Perona and Malik [21] is performed on the posterior probability matrix of each class in order to reduce the influence of speckle. The prior information required by AD is automatically introduced by MAP which is part of the whole segmentation process; in this sense, the whole process can be regarded unsupervised.

The paper is organized as follows. In Section 2 the relationship between the solid heat diffusion model and image scale-space is described. In Section 3 our segmentation method of SAR images is presented in detail. In Section 4 some test results from a set of simulated and real data are given. Also, the proposed algorithm is compared with a MRF-based method in terms of accuracy and consumed time, and the limitations and extensive application of the presented algorithm in this study are discussed. Finally, some main conclusions of this investigation are summarized.

2. The solid heat diffusion model and image scale-space

In recent years, algorithms based on the PDE derived from the solid heat diffusion model have shown remarkable performance in image processing tasks such as noise removal, image enhancement, segmentation, etc. This type of method has

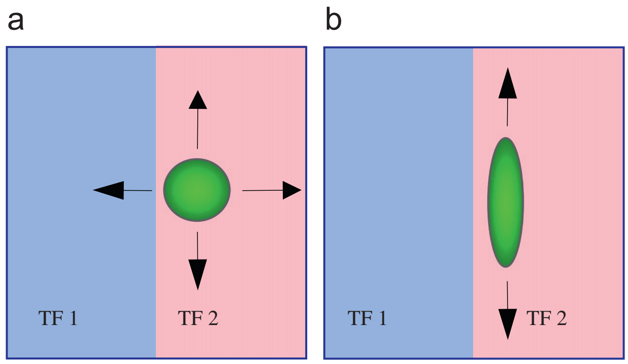

Fig. 1. Solid heat diffusion: (a) isotropic; (b) anisotropic. TF represents temperature field.

the advantage of preserving important structure information in the image while simultaneously denoising the image. The solid heat diffusion model is described as follows. Suppose that u is the temperature field of Ω in plane medium and Q is the heat energy. The energy Q varies with time t as [22]

$$\frac{\mathrm{d}Q}{\mathrm{d}t} = \iint_{\partial\Omega} \sigma \vec{n} \cdot \nabla u(t, x)\, \mathrm{d}^2 x \tag{1}$$

where $\vec{n}$ is the normal vector of the region boundary $\partial\Omega$, ∇u is the gradient field of u, σ is heat conductivity, and x represents location of point in the plane. According to the conservation of energy and divergence law, Eq. (1) is rewritten as

$$\frac{\mathrm{d}Q}{\mathrm{d}t} = \iiint_{\Omega} \nabla\sigma\nabla u(t, x)\, \mathrm{d}^3 x \tag{2}$$

Combining Eq. (1) with Eq. (2), the heat diffusion equation is

$$u_t(t, x) = \frac{\partial u(t, x)}{\partial t} = \mathrm{div}(c(x, y, t) \cdot \nabla u(t, x)) \tag{3}$$

where $\mathrm{div}(\cdot)$ is the divergence operator and $c(x, y, t)$ represents the diffusion coefficient. In the isotropic medium $c(x, y, t)$ is a constant. Fig. 1 shows two typical cases of solid heat diffusion.

If we regard the value of each point in the temperature field as a gray level value in an image, heat diffusion becomes image smoothing. Koenderink [23] and Hummel [24] point out that convolving an image I_0 with a Gaussian filter G_σ is equivalent to the solution of the standard diffusion equation

$$\frac{\partial I}{\partial t} = \Delta I; \quad I|_{t=0} = I_0 \tag{4}$$

where t becomes the scale parameter and $\Delta(\cdot)$ is the Laplacian operator. Scale space is thus related with the solid heat diffusion equation. Eq. (4) is essentially an isotropic diffusion equation. Perona and Malik [21] considers that important feature can be preserved while denoising if a proper AD equation is constructed. Furthermore, Haker et al. [12] point out that images with multiplicative noise can also be denoised in this way.

3. Algorithm details

3.1. The initial segmentation

Image segmentation can be viewed as the problem of partitioning the image into different connected regions. Each region is identified by a unique label. Let us consider a rectangular pixel lattice $S = \{s = (i, j), 1 \leqslant i \leqslant M, 1 \leqslant j \leqslant N\}$, where $s = (i, j)$ denotes the coordinate of a point in the $M \times N$ image. $I = \{I_s; s \in S\}$ represent the corresponding intensity image. After segmentation we can get a label image $X = \{x_s; s \in S, x_s \in \{1, 2, \ldots, p\}\}$, where p denotes the number of different regions and is given in advance. Each region can be regarded as a class.

Based on the coherent imaging mechanism, it is well known that the negative exponential distribution provides a good model for single-look SAR intensity data [1]. Therefore, we suppose that each pixel belonging to class m in the SAR image satisfies negative exponential distribution [8] (the iterating processing in this section can also be used to other distributions). Formally

$$f(I_s|x_s = m; 1 \leqslant m \leqslant p) = \frac{1}{\sigma_m} \exp\left\{-\frac{I_s}{\sigma_m}\right\} \tag{5}$$

where σ_m is the parameter of negative exponential distribution associated with class m. According to Bayes' rule, the posterior probability is

$$P(x_s = m|I_s) = \frac{f(I_s|x_s = m)P(x_s = m)}{\sum_{i=1}^{p} f(I_s|x_s = i)P(x_s = i)} \tag{6}$$

Given the intensity value I_s of pixel s, the segmentation is equivalent to the MAP optimal solution,

$$\hat{x}_s = \arg \max_{x_s \in \{1,2,\ldots,p\}} \{P(x_s|I_s)\} \tag{7}$$

Eq. (7) gives a form of initial segmentation, which is an iterative and pixel-intensity-based scheme. After each iteration, distribution parameters should be re-estimated as

$$(\hat{\sigma}_m^{i+1}; 1 \leqslant m \leqslant p) = \arg \max_{\sigma_m} \prod_{\hat{x}_s^i = m} P(I_s|\hat{x}_s^i) \tag{8}$$

The initial parameter σ_m^0 can be estimated as follows: the pixels in the image are ranked according to their intensity; the ranked pixels are equally divided into p sets and σ_m^0 $(1 \leqslant m \leqslant p)$ is assigned the mean of the mth set. For a real scene, the priori probability of each class $P(x_s)$ is unknown. So we assume the same probability for a pixel belonging to each class $(P(x_s = m) = 1/p)$. After each iteration, the current posterior probability that a pixel belongs to class m is computed and used as the prior probability of the pixel belonging to class m for the next iteration. The convergence of the segmentation is reached when $\hat{\sigma}_m^i$ and $\hat{\sigma}_m^{i+1}$ are almost equal (in our experiments, we regard that the algorithm get convergence when $|\hat{\sigma}_m^{i+1} - \hat{\sigma}_m^i| \leqslant 0.01$). So we can summarize the initial segmentation process as three steps:

1. Supposing $P(x_s = m) = 1/p$, the initial distribution parameters of each class are estimated.

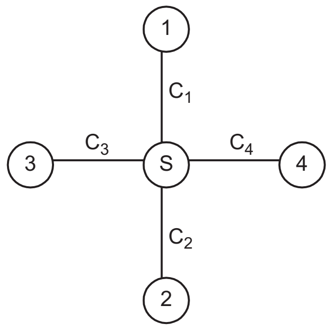

Fig. 2. Four neighbors of a pixel.

2. After ith iteration, we compute the distribution parameters of each class for $i+1$th iteration according to current segmentation result by Eq. (8). The posterior probability that a pixel belongs to class m is also computed and used as the prior probability of the pixel belonging to class m at $i+1$th iteration.
3. Repeat step 2 until the convergence of the segmentation is reached.

3.2. Speckle removing

The initial segmentation is a method based on pixel intensity and cannot reduce the influence of speckle. So we use multiscale anisotropic smoothing of the posterior probability matrix to remove the speckle. Let $P^m = \{P^m(s);\ s \in S\}$ represent the posterior probability matrix of class m after the initial segmentation, and $P^m(s)$ be the posterior probability of pixel s belonging to class m. As pointed out in Section 2, the smoothing of posterior probability matrix is equivalent to solving the anisotropic PDE [21]

$$\frac{\partial P^m}{\partial t} = \mathrm{div}(c(|\nabla I|) \cdot \nabla I) \tag{9}$$

where $\nabla(\cdot)$ is the gradient operator, and $|\cdot|$ denotes the magnitude. We consider the four nearest neighbors of a pixel (see Fig. 2) and use the discrete form of Eq. (9). Then the solution in an iterative form of Eq. (9) can be written as

$$P_s^{t+1,m} = P_s^{t,m} + \frac{1}{|\overline{\eta}_s|} \sum_{l \in \overline{\eta}_s} c(\nabla P_{s,l}^{t,m}) \nabla P_{s,l}^{t,m} \tag{10}$$

where $\overline{\eta}_s$ denotes the neighborhood of pixel s, $|\overline{\eta}_s|$ is the number of pixels in $\overline{\eta}_s$, $P_s^{t,m}$ is the posterior probability of pixel s belonging to class m at iteration t, $\nabla P_{s,l}^{t,m} = P_l^{t,m} - P_s^{t,m}$. According to the selection strategy in Ref. [21], we have

$$c(\nabla P^m) = \exp(-(\|\nabla P^m\|/K)^2) \tag{11}$$

where the constant K is a threshold of the edge strength map and fixed either by hand at some fixed value [21], or estimated by the method described by Canny [25]: a histogram of the absolute values of the gradient throughout the image is computed, and K is set equal to the 90% value of its integral at every iteration. $\|\cdot\|$ is the norm operator.

Let $\overline{P}_T^m = \{\overline{P}_T^m(s);\ s \in S\}$ be the posterior probability matrix after smoothing P^m with scale parameter T, and $\overline{P}_T^m(s)$ represent the posterior probability that pixel s belongs to class m after smoothing. Then the final segmentation result is

$$\hat{x}_s = \arg \max_{1 \leqslant m \leqslant p} \overline{P}_T^m(s); \quad s \in S \tag{12}$$

4. Experiment

4.1. The experiment results

The proposed segmentation method is applied to simulated and real SAR images.

We begin with an 128×128 artificial image consisting of three regions with different intensity values (Fig. 3(a)). The effects of speckle are simulated by using a Gaussian random number generator to produce a speckle image of the same size as the artificial image. Since speckle noise is multiplicative, the artificial image is multiplied by the speckle image pixel by pixel. In order to evaluate the quality of each region in the image, we use the concept of signal-to-noise (SNR) defined as

$$SNR = 20 \log_{10} \left(\frac{\overline{I}}{\sigma} \right) \tag{13}$$

where $\overline{I}$ is the average intensity of a region and σ is the standard deviation of noise. The SNR of each region in Fig. 3(b) is 0 dB, which is a low SNR level. The initial segmentation result is shown in Fig. 3(c). As we can see, this result is not satisfactory because there are a large number of “false alarms” in each region due to the speckle noise. The initial segmentation utilizes only the intensity information of the tested image, so it cannot remove the influence of speckle noise. Fig. 3(d) is the final segmentation result with the scale parameter $T = 15$. We can clearly see that an acceptable segmentation result compared with the original image shown in Fig. 3(a) is obtained although the SNR level of the corresponding SAR image is low. Furthermore, Fig. 3(d) also shows that the proposed method has the ability to preserve the structure information of the image.

A set of MSTAR SAR images [20] has also been tested. It contains SAR images of three types of vehicles, namely T72 (1273 images), BMP2 (1284 images), and BTR70 (429 images). Taking Fig. 4(a) for example, it shows an original SAR image of T72 with the radar’s depression angle of 15° and the target’s orientation angle of 240.79°. This image mainly contains three regions: background, target, and shadow. In the test images three regions (shadow, target, and background) are quite distinct from one another (see Fig. 4). We define each region in the images manually and compare them with the results of the proposed method. The pixels belonging to target or shadow in the experiment results while belonging to background in the manual segmentation are defined as false positives. Fig. 4(b) is the initial segmentation result. There are many false alarms in the initial segmentation result. Gaps and holes exist in both target and shadow regions. Fig. 4(c) is the final segmentation result with the scale parameter $T = 7$. In Fig. 4(c) we find fewer false alarms than those in Fig. 4(b). Fig. 4(d) shows a

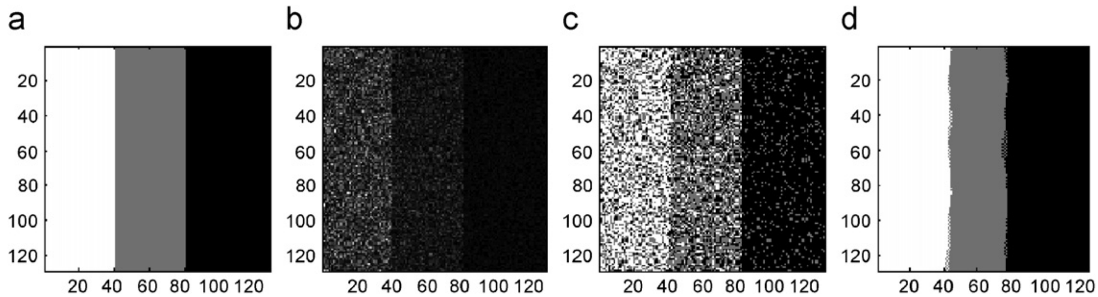

Fig. 3. The experiment of a simulated SAR image: (a) original image; (b) the simulated SAR image (SNR $= 0$ dB) by adding the multiplicative noise to (a); (c) the initial segmentation; (d) the final segmentation.

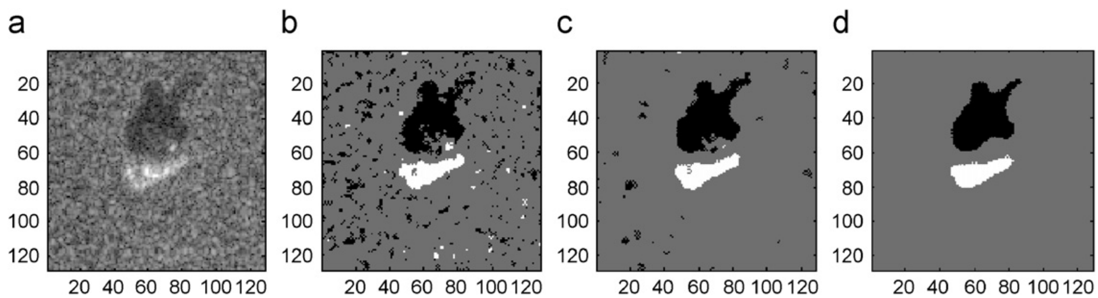

Fig. 4. The segmentation result of a real SAR image: (a) original image; (b) the initial segmentation; (c) the final segmentation result ($T = 7$); (d) the final segmentation result ($T = 11$).

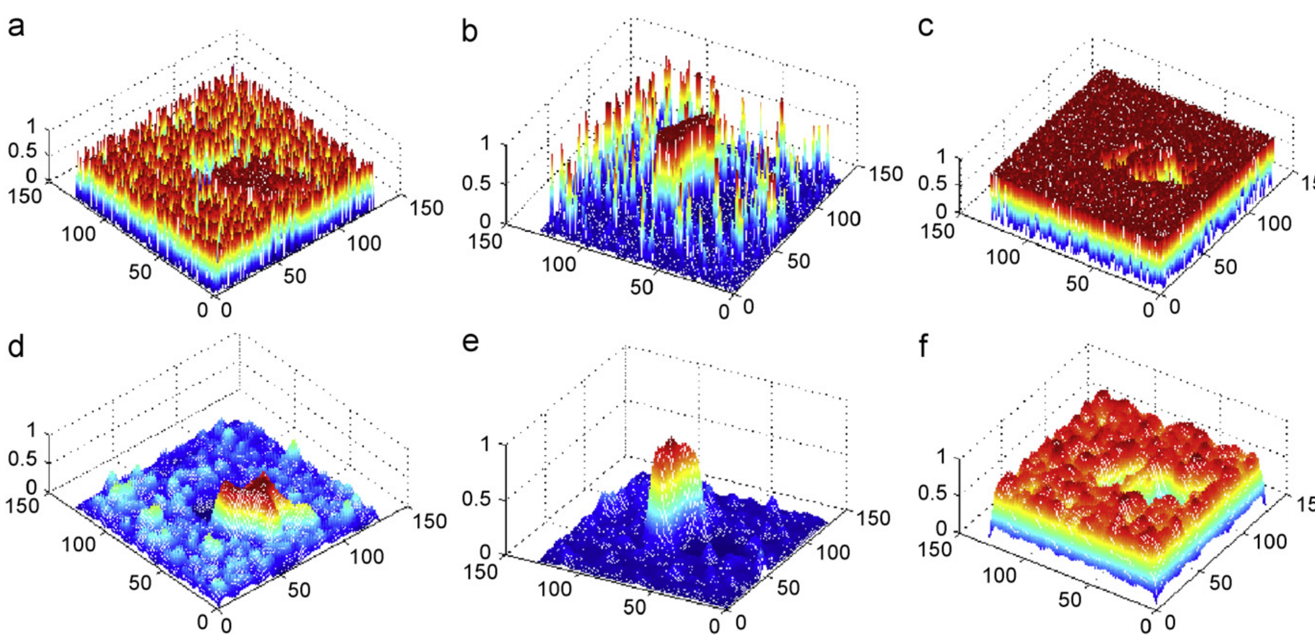

Fig. 5. The posterior probability plots of the initial segmentation and the final segmentation: (a), (b), and (c) correspond to the posterior probability plots of the initial segmentation of shadow, target, and background, respectively; (d), (e), and (f) correspond to those of the final segmentation of shadow, target, and background, respectively.

more satisfactory segmentation result with the scale parameter $T = 11$. The number of false alarms drops to zero.

According to the initial segmentation (Fig. 4(b)), the posterior probability plots of shadow, target, and background are, respectively, shown in Fig. 5(a)–(c). Fig. 5(d)–(f), respectively, correspond to the posterior probability plots of shadow, target, and background based on final segmentation in Fig. 4(d). We can find that our method has a good performance of removing false alarms and suppressing speckle.

We use 2986 SAR images in MSTAR dataset for further analyzing the performance of our method. Firstly, the change pattern of the average number of false alarms in each region

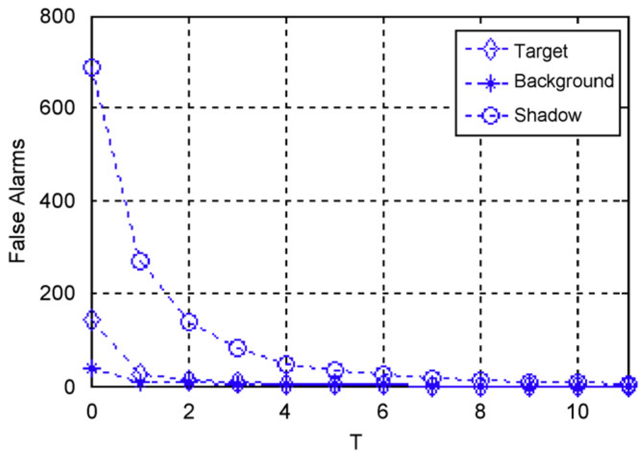

Fig. 6. The curves of the number of false alarms varying with the scale parameter.

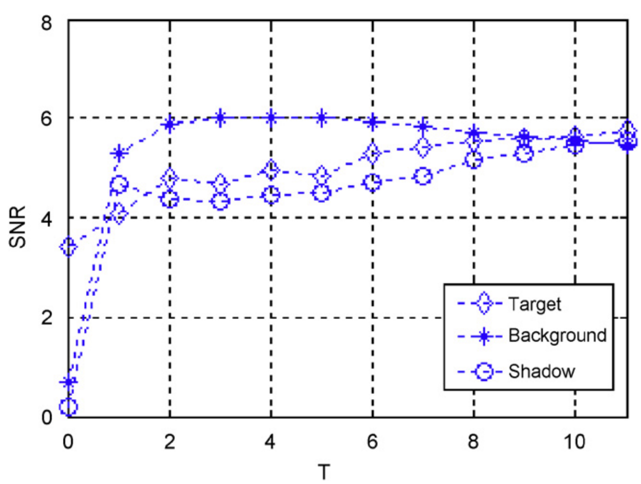

Fig. 7. The curves of the SNR values of each region varying with the scale parameter.

(target, background, and shadow) with respect to the scale parameters is considered and corresponding curves are shown in Fig. 6. We find that the average number of false alarms in each region all has a descending tendency when the scale parameter increases. Moreover, if the scale parameter $T \geqslant 11$, false alarms due to speckle can be removed.

In order to verify the ability of our method to suppress the speckle and to enhance the signal, the SNR of each region in the initial segmentation result ($T = 0$) and in the final results with different scale parameters are computed for each tested image. Fig. 7 shows the performance curves of the average SNR values in each region varying with the scale parameters. It shows that the SNR value of each region gradually increases when the scale parameter increases and quickly converges, which verifies the effect of speckle suppression and signal enhancement of this algorithm. When the scale parameter $T > 6$, it also can be found in Fig. 7 that the SNR value about the background region has a slightly descending tendency with the increase in the scale parameter. Conversely, the SNR values corresponded to

Table 1
The testing results of the images of different targets using our algorithm

	T72	BMP2	BTR70
The number of target's images	1273	1284	429
The average scale without false alarm	10.76	11.12	10.87
The average time in our algorithm (s)	4.39	4.28	4.27

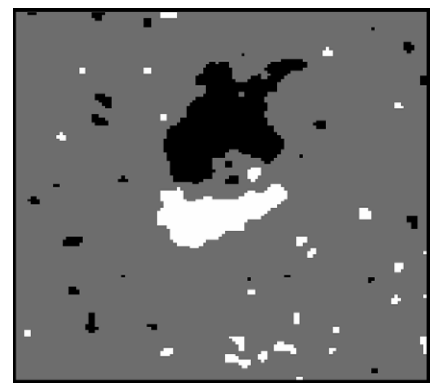

Fig. 8. The segmentation result by applying the algorithm presented in literature [8] to Fig. 4(a).

the target region and the shadow region tend to be stable. The reason is as follows: when the scale parameter T increases, the pixels due to the loss of target and shadow information are confused with the background region and make the corresponding SNR value decline.

All the experiments are accomplished in MATLAB code with a hardware environment of PIII 500M CPU and 512M memory. Table 1 presents the testing results by applying our algorithm to three kinds of targets in MSTAR dataset. It is evident that the segmentation results have zero false alarm for real MSTAR SAR images when the scale parameter is about 11. The average time of the speckle filtering approach based on AD in this study for one MSTAR image is about 3.13 s. Meanwhile, the time consumed for the segmentation of each image is less than 4.5 s.

4.2. Comparison with the MRF-based algorithm

A typical method used for SAR image segmentation is the MRF-based one, which usually has a high accuracy at the cost of a low speed. We compare our method with the MRF-based one presented in Ref. [8]. Fig. 8 shows the segmentation result of Fig. 4(a) by applying the algorithm in Ref. [8] with the number of iterations set to 100. For a direct and visual estimation, the segmentation result of the MRF-based algorithm is not as good as that of our method with the scale parameter 11.

Since there is no a priori knowledge of the extract location of the segmentation boundaries, manual segmentation is assumed to give the best fit in this study. In general, the actual position of boundaries within a SAR scene is unknown. So, the goodness measures are modified to compare the segmentation approaches with manual segmentation. In this investigation, assuming that the size of an original SAR image is $M \times N$, we denote the label image obtained by segmentation as $\hat{X} = \{\hat{x}_s; s \in S, \hat{x}_s \in \{1, 2, \ldots, p\}\}$, whose size is also $M \times N$. Correspondingly, R represents the label image from manual segmentation for the same original SAR image. Moreover, the error image is defined as $E = \hat{X} - R$. In order to compare the performance of the above mentioned two methods, a measurement which evaluates the accuracy of segmentation, called the percent of error pixels (*pep*), is defined by us as

$$pep = \frac{l}{M \times N} \times 100\% \tag{14}$$

where l denotes the number of non-zero pixels in E. Ideally, the *pep* value of a perfect segmentation should be equal to zero, and the closer *pep* is to zero, the better the segmentation is. Therefore, this measurement indicates the quality of the image segmentation. We compute the *pep* values using the results of three kinds of targets in MSTAR dataset by our method and the MRF-based one in Ref. [8], respectively. The method in Ref. [8] is also accomplished in MATLAB code and run on the same CPU and memory as this paper's method. Then, the average measure of accuracy of each kind of target is obtained by dividing the sum of the *pep* values of corresponding target kind by the number of the targets.

Table 2 compares the two methods in accuracy and speed. We can see that our method is faster and more accurate than that presented in Ref. [8].

4.3. Discussion and extensive application

Much work remains to be done in future before the proposed method can be used in a practical system. Although experiments have testified that our method has a better performance than using a method based on MRF, it is not entirely unsupervised since a priori knowledge of the number of classes p in segmenting SAR images is required. Furthermore, an optimum choice of the scale parameter T of the anisotropic smoothing is currently a problem under study. As discussed in Section 4.1, when the scale parameter T increases, the false positives caused by speckle can be removed. But the increase in T will also lead to loss of target and shadow information (see Fig. 4). So how to automatically select T is an important issue. So far we have no theoretical solution to this problem. We have also attempted to find out whether T has a relationship with the size of the targets and the spatial resolution of images or not. However, after utilizing many different targets, we still find no apparent relationship between them. Maybe not only the targets' size or the spatial resolution is related, but also the quality of image such as SNR is also related with the choice of T. In actual application, the empirical choice of T is needed.

Over the last few years, information extraction from SAR images is still an active research area for many operational SAR sensors that are becoming available in the very near future [9,14,15,26]. The presented segmentation algorithm is used to extract the water area in real SAR images. In this investigation, the extraction of water area from SAR images uses a hierarchical process, which has three stages: (1) the image is segmented to separate dark region and extract approximate contour of water area as the initial contour; (2) snake model based on gradient vector flow [27] is used to obtain more accurate contour on the basis of the initial contour; (3) some small regions are eliminated.

The experiment data were collected by an air-borne SAR platform in the year of 2007. The dataset with 6 m × 6 m resolution includes 50 scenes that contain different water areas in China. The air-borne SAR platform operated at X-band and collected data in stripmap mode with HH polarization.

As a direct and visual example, Fig. 9(a) shows a test SAR image containing Wujiang river, in China. The image size is 1665 rows and 1665 columns. The segmentation image using our algorithm is shown in Fig. 9(b). According to the application of extracting the water area, we think that the radar returns of objects are dominated approximately by three kinds of

Table 2
The comparison between two algorithms

Target	The algorithm in literature [8]		Our algorithm	
	Average *pep* (%)	Average time (s)	Average *pep* (%)	Average time (s)
T72	3.53	16.3814	0.61	4.39
BTR70	3.27	16.2175	0.54	4.27
BMP2	3.39	16.1732	0.56	4.28

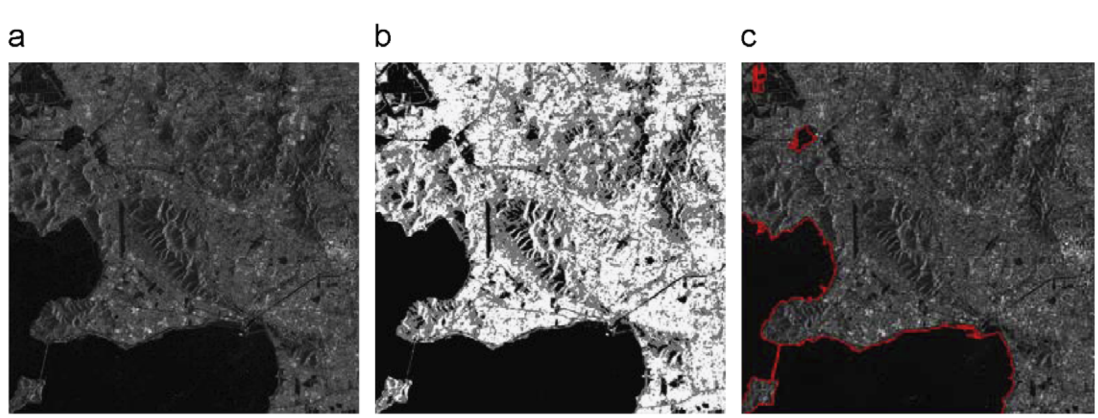

Fig. 9. The result of extracting water areas in a test SAR image. (a) Original SAR image; (b) the result of segmentation; (c) the result of extracting water areas.

scattering mechanisms. The river represents the weakest scattering. Therefore, the number of classes p in segmenting SAR images is 3. For all scenes in this application, we find that the good segmentation can be obtained by setting T around 10. So the choice of T is empirically justified. Fig. 9(c) shows the extracting result of corresponding water area in Fig. 9(a). As we can see, the contours of the water regions are extracted accurately. Although some of the choices are empirical, it is apparent that the presented segmentation algorithm is applied successfully to water area extraction.

5. Conclusion

Segmentation is a key step in SAR image interpretation. A new segmentation for SAR images combining MAP and AD is proposed in this study. An initial segmentation is obtained by MAP using intensity information of pixels, then multiscale anisotropic smoothing is implemented on the posterior probability matrixes derived from the initial segmentation. The segmentation results of simulated and real SAR images show the feasibility and efficiency of our method. The technique proposed in this study can be improved by smoothing the posterior probability matrixes by the work of Yu and Acton [17] or other AD filters [19,28,29]. More experiments will also be done by using more real SAR data to find the selection of the value T in our further work.

Acknowledgments

The authors would like to thank all the reviewers for providing several important suggestions for improving the paper, and also, the authors acknowledge the patience and time of the editors for processing this manuscript.

References

[1] C.J. Oliver, S. Quegan, Understanding SAR Images, Artech House, New York, 1998.
[2] R. Meth, Target characterization and matching in synthetic aperture radar imagery, Doctor's dissertation, The University of Maryland, College Park, 1998.
[3] C.H. Fosgate, H. Krim, W.W. Irving, W.C. Karl, A.S. Willsky, Multiscale segmentation and anomaly enhancement of SAR imagery, IEEE Trans. Image Process. 6 (1) (1997) 7–20.
[4] H. Choi, R.G. Baraniuk, Multiscale image segmentation using wavelet-domain hidden Markov models, IEEE Trans. Image Process. 10 (9) (2001) 1309–1321.
[5] R. Cook, I. McConnell, MUM (merge using moments) segmentation for SAR images, SPIE SAR Data Processing for Remote Sensing, vol. 2316, 1994, pp. 92–103.
[6] R. Cook, I. McConnell, D. Stewart, Segmentation and simulated annealing, SPIE Microwave Sensing and Synthetic Aperture Radar, vol. 2958, 1996, pp. 30–37.
[7] R.A. Weisenseel, W.C. Karl, D.A. Castanon, G.J. Power, P. Douville, Markov random field segmentation methods for SAR target chips, SPIE Algorithms for Synthetic Aperture Radar Imagery VI, vol. 3721, 1999, pp. 19–27.
[8] R.A. Weisenseel, W.C. Karl, D.A. Castanon, R.C. Brower, MRF-based algorithms for segmentation of SAR images, IEEE Proceeding of the 1998 International Conference on Image Processing, vol. 3, 1998, pp. 770–774.
[9] H. Deng, D.A. Clausi, Unsupervised segmentation of synthetic aperture radar sea ice imagery using a novel Markov random field model, IEEE Trans. Geosci. Remote Sensing 43 (3) (2005) 528–538.
[10] J. Besag, On the statistical analysis of dirty pictures, J. R. Stat. Soc. B 48 (1986) 259–302.
[11] D. Stewart, D. Blacknell, A. Blake, R. Cook, C. Oliver, Optimal approach to SAR image segmentation and classification, IEE Proc. Radar Sonar Navigation 147 (3) (2000) 134–142.
[12] S. Haker, G. Sapiro, A. Tannenbaum, Knowledge-based segmentation of SAR data with learned priors, IEEE Trans. Image Process. 9 (2) (2000) 299–301.
[13] Y. Cao, H. Sun, X. Xu, An unsupervised segmentation method based on MPM for SAR images, IEEE Geosci. Remote Sensing Lett. 2 (1) (2005) 55–58.
[14] P. Lombardo, C.J. Oliver, Optimal classification of polarimetric SAR images using segmentation, in: IEEE Radar Conference 2002, Long Beach (CA), 2002, pp. 8–13.
[15] P. Lombardo, C.J. Oliver, Optimal polarimetric segmentation for the classification of agricultural areas, EUSAR 2002, Koeln, Germany, June 2002.
[16] P. Lombardo, C.J. Oliver, Optimum detection and segmentation of oil-slicks using polarimetric SAR data, IEE Proc. Radar Sonar Navigation 147 (6) (2000) 309–321.
[17] Y. Yu, S.T. Acton, Speckle reducing anisotropic diffusion, IEEE Trans. Image Process. 11 (11) (2002) 1260–1270.
[18] T.T. Georgiou, A. Tannenbaum, High resolution sensing and anisotropic segmentation for SAR imagery, in: Proceedings of the 2000 IEEE Conference on Decision and Control, Sydney, December 2000, pp. 4324–4326.
[19] S. Aja-Fernández, C. Alberola-López, On the estimation of the coefficient of variation for anisotropic diffusion speckle filtering, IEEE Trans. Image Process. 15 (9) (2006) 2694–2701.
[20] MSTAR Targets T72, BMP2, BTR70, SLICY, Available at: ⟨http://www.mbvlab.wpafb.af.mil/public/MBVDATA/⟩, 1997 (Online).
[21] P. Perona, J. Malik, Scale-space and edge detection using anisotropic diffusion, IEEE Trans. Pattern Anal. Mach. Intell. 12 (7) (1990) 629–639.
[22] M. Evans, Harrell II, J.V. Herod, Linear Methods of Applied Mathematics, ⟨www.mathphysics.com/pde⟩.
[23] J. Koenderink, The structure of images, Biol. Cybern. 50 (1984) 363–370.
[24] R.A. Hummel, Representations based on zero-crossings in scale-space, in: IEEE Proceedings of Computer Society Conference on Computer Vision and Pattern Recognition, 1986, pp. 204–209.
[25] J. Canny, A computational approach to edge detection, IEEE Trans. Pattern Anal. Mach. Intell. 8 (1986) 679–698.
[26] P.T. Macri, C.J. Oliver, P. Lombardo, Segmentation-based joint classification of SAR and optical images, IEE Proc. Radar Sonar Navigation 149 (6) (2002) 281–296.
[27] C. Xu, J.L. Prince, Snakes, shapes, and gradient vector flow, IEEE Trans. Image Process. 7 (3) (1998) 359–369.
[28] K.Z. Abd-Elmoniem, A.M. Youssef, Y.M. Kadah, Real-time speckle reduction and coherence enhancement in ultrasound imaging via nonlinear anisotropic diffusion, IEEE Trans. Biomed. Eng. 49 (9) (2002) 997–1014.
[29] F. Zhang, Y.M. Yoo, L.M. Koh, Y.M. Kim, Nonlinear diffusion in Laplacian pyramid domain for ultrasonic speckle reduction, IEEE Trans. Med. Imaging 26 (2) (2007) 200–211.

About the Author—GUI GAO, male, born in 1981, Ph.D., a lecturer of National University of Defence Technology. His main research interests include SAR image interpretation and SAR ATR.

About the Author—LINGJUN ZHAO, female, born in 1981, Ph.D. Her main research interests include SAR building detection and SAR image segmentation.

About the Author—DIEFEI ZHOU, female, born in 1981, Master. Her main research interests include SAR ATR and SAR image processing.

About the Author—JUN ZHANG, female, born in 1975, Ph.D., Associate Professor. Her main research interests include GIS spatial modeling, the information processing of remote sensing and SAR image interpretation.

About the Author—JIJUN HUANG, male, born in 1971, Ph.D., Associate Professor. His main research interests include UWB-SAR imaging, and target detection.